Nonlinear threshold behavior during the loss of Arctic sea ice

I. Eisenman[1] & J.S. Wettlaufer[2]

The rapid retreat of Arctic sea ice during recent decades[1] is believed to be augmented by the difference in albedo (i.e., reflectivity) between sea ice and exposed ocean waters[2]. Because bare or snow-covered sea ice is highly reflective to solar radiation, the increasing area of open water that is exposed as sea ice recedes leads to an increase in absorbed solar radiation, thereby contributing to further ice retreat. In light of this positive ice-albedo feedback, the possibility that retreating sea ice might cross a critical bifurcation threshold (or "tipping point") after which it would melt back on an irreversible trajectory to a second stable state that is at least seasonally ice-free[3–10] has emerged as a key issue. Here we show that while the ice-albedo feedback promotes the existence of multiple sea ice cover states, the stabilizing thermodynamic effects of sea ice mitigate this when the Arctic Ocean is ice-covered during a sufficiently large fraction of the year. These results suggest that nonlinear threshold behavior is unlikely during the approach from current perennial sea ice conditions to seasonally ice-free conditions. In a further warmed climate, however, we find that the a bifurcation threshold associated with the sudden loss of the remaining wintertime-only sea ice cover may be likely.

Heuristically, one might expect in a simple annual mean picture of the Arctic Ocean that completely ice-covered and ice-free stable states could co-exist under the same climate forcing. The ice-free state would remain warm due to the absorption of most incident solar radiation, whereas the ice-covered state would reflect most solar radiation and remain below the freezing temperature. In such a picture, the two stable states would be separated by an unstable intermediate state in which the Arctic Ocean is partially covered by ice and absorbs just enough solar radiation to remain at the freezing temperature: adding a small amount of additional sea ice to this unstable state would lead to less solar absorption, cooling, and a further extended sea ice cover. If the background climate warmed, the unstable state would require an increased ice extent to reflect sufficient solar radiation to remain at the freezing temperature. Beyond a critical threshold, the background climate would become so warm that the ocean would not be able to remain below the freezing point even when the entire domain had the low surface albedo characteristic of ice. At this point the stable ice-covered state and unstable intermediate state would merge and disappear in a saddle-node bifurcation, leaving only the warm ice-free state[11–13]. This scenario suggests that if an ice-covered Arctic Ocean were warmed beyond the bifurcation point, there would be a rapid transition to the ice-free state. It would be an irreversible process, to the extent that the Arctic Ocean would only refreeze after the climate had cooled to a second bifurcation point at which even an ice-free Arctic Ocean would become cold enough to freeze, representing a significantly colder background climate than the original point at which the ice disappeared.

Here we investigate the central physical processes underlying the possibility of such a bifurcation threshold in future sea ice retreat. We illustrate the discussion with a seasonally varying model of the Arctic sea ice–ocean–atmosphere climate system which is derived from basic physical principles. The theory produces an observationally consistent simulation of the modern Arctic sea ice seasonal cycle using a single one-dimensional nonautonomous ordinary differential equation. A brief summary of the model equations is presented below (see full model derivation in Supplementary Methods section).

The state variable E represents the energy per unit area stored in sea ice as latent heat (when the ocean is ice-covered) or in the ocean mixed layer as sensible heat (when the ocean is ice-free),

$$E \equiv \begin{cases} -L_i h & E < 0 \text{ [sea ice]} \\ c_{ml} H_{ml} T_{ml} & E \geq 0 \text{ [ocean]} \end{cases}, \qquad (1)$$

with L_i the latent heat of fusion for sea ice, c_{ml} the mixed layer specific heat capacity, and H_{ml} the mixed layer depth. The theory presented here describes the thermal evolution of sea ice, ocean mixed layer, and an energy balance atmosphere that is in steady-state with the underlying surface forcing, including also representations of dynamic sea ice export and diffusive atmospheric meridional heat transport. The evolution of E is given as

$$\frac{dE}{dt} = [1-\alpha(E)]\, F_S(t) - F_0(t) - F_T(t) T(t,E) + F_B + v_0 \mathcal{R}(-E), \qquad (2)$$

where the surface temperature, written in terms of departure from the freezing point, is given by

$$T(t,E) = \begin{cases} -\mathcal{R}\left[\frac{F_0(t)-(1-\alpha_i)F_S(t)}{F_T(t)-k_i L_i/E}\right] & E < 0 \text{ [sea ice]} \\ \frac{E}{c_{ml} H_{ml}} & E \geq 0 \text{ [ocean]} \end{cases} \qquad (3)$$

in which the ramp function, $\mathcal{R}(x)$, is equal to x when $x \geq 0$ and equal to 0 when $x < 0$, and the surface albedo is ex-

[1] *Department of Earth & Planetary Sciences, Harvard University, Cambridge, Massachusetts, USA*
[2] *Department of Geology & Geophysics and Department of Physics, Yale University, New Haven, Connecticut, USA*

pressed as

$$\alpha(E) = \frac{\alpha_{ml} + \alpha_i}{2} + \frac{\alpha_{ml} - \alpha_i}{2} \tanh\left(\frac{E}{L_i h_\alpha}\right). \quad (4)$$

At any time, the ocean is represented as either ice-covered or ice-free. Hence to approximately account for the gradual transition between these regimes in a partially ice-covered Arctic Ocean, the model albedo varies between values for ice (α_i) and ocean mixed layer (α_{ml}) in equation (4) with a characteristic smoothness given by h_α. The surface heat flux is determined by $F_0(t)$ and $F_T(t)$, which represent a linearization of the Stefan-Boltzmann equation for outgoing longwave radiation with a partially opaque atmosphere, also including the effects of atmospheric heat flux convergence that depends on the meridional temperature gradient. Their seasonally varying values are specified using an atmospheric model that incorporates observations of Arctic cloudiness[14], surface air temperature south of the Arctic[15], and atmospheric heat flux convergence in the Arctic[16]. Shortwave radiation $F_S(t)$ and basal heat flux F_B are specified at central Arctic values[17], and an observationally-based constant ice export of v_0 =10% per year is included[18].

The sea ice thermodynamics in this model are an approximation of the full heat conduction equation of Maykut & Untersteiner[17], which provides the thermodynamic basis for most current sea ice models. Ice grows during the winter at the base, and in summer when the surface reaches the melting temperature ablation occurs at the surface as well as at the base. The surface temperature (3) is calculated for sea ice ($E < 0$) based on the balance between upward heat flux in the ice (which involves the ice thermal conductivity k_i) and the heat flux above the ice surface. The ramp function $\mathcal{R}(x)$ provides a convenient notation for combining an equation for temperatures above the freezing point with a separate equation for temperatures below the freezing point.

We also consider a linearized ice version of the model in which equation (3) is replaced with

$$T(t, E) = \frac{E}{c_{ml} H_{ml}}, \quad (5)$$

and there is no ice export ($v_0 = 0$). This causes the model equations to be linear with the exception of the ice-albedo feedback (4).

In a seasonally varying Arctic climate, warming would be expected to cause the sea ice to initially melt back to the point where the entire Arctic Ocean is ice-free during part of the year, in contrast to the current perennial sea ice cover in the central Arctic. Further warming would cause the ice-free period to increase until the Arctic Ocean becomes perennially ice-free. We study this scenario by prescribing a warming in the model (equations (2)-(4)) through addition of an annually constant term ΔF_0 to the seasonally varying surface flux $F_0(t)$. In Fig. 1a, steady-state solutions are plotted in regimes with perennial ice cover (blue curve), partial-year ice cover (red curves), and perennial ice-free conditions (black curve).

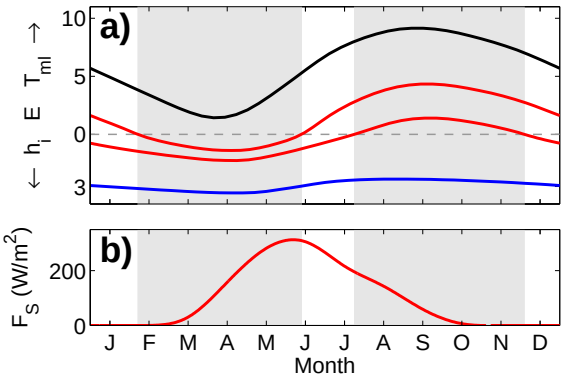

Figure 1: (a) Seasonal cycle of stable solutions of the full nonlinear model. Model state E is plotted versus time of year, with numbers on the vertical axis indicating ice thickness (m) when $E < 0$ and mixed layer temperature (°C) when $E > 0$ according to equation (1). Note that ice thickness increases downward. Four solutions are plotted, each with different levels of surface heating: a perennial ice state (blue curve, $\Delta F_0 = 0$), seasonally ice-free states with most of the year ice-covered (lower red curve, $\Delta F_0 = 21$ W/m^2) or most of the year ice-free (upper red curve, $\Delta F_0 = 23$ W/m^2), and a perennial open water state (black curve, $\Delta F_0 = 19$ W/m^2). Note that this system can support multiple stable states, and the black curve representing the warm state is forced by a smaller value of ΔF_0 than the red curves which represent the cold state (cf. Fig. 2b). (b) Seasonal cycle of specified incident solar radiation.

The annual minimum sea ice area and thickness is commonly referred to as "summer" sea ice and the annual maximum is commonly referred to as "winter" sea ice. This nomenclature may carry with it the implication that the ice-albedo feedback would be most prominent during the retreat of the summer sea ice cover. Indeed, it is often conjectured that a critical threshold for the loss of summer Arctic sea ice may be more likely than a threshold for the loss of winter ice[19]. However, as is illustrated by Fig. 1b, this terminology can be misleading because the ice cover receives a similar amount of solar radiation during the period of annual minimum as at annual maximum. The gray shaded regions in Fig. 1 illustrate the key transition periods in the state of the Arctic Ocean during the transition from perennial to partial-year ice cover (gray region to right) and from partial-year ice cover to perennial ice-free conditions (gray region to left). Both of these periods experience roughly equivalent amounts of incident solar radiation (Fig. 1b), with somewhat more solar radiation occurring during the period associated with the loss of winter ice (gray region to left). Hence the ice-albedo feedback should be expected to be similarly strong during a distant transition to perennial ice-free conditions as during a more imminent possible warming to seasonally ice-free conditions.

Next, we use the linearized ice version of the model

(equations (2), (4)-(5)) to focus on the effect of albedo in the absence of other nonlinearities. In this representation, the Arctic Ocean is viewed as a simple radiating thermal reservoir with a temperature-dependent albedo, and the model exhibits a constant linear relaxation to stable solutions in each albedo regime. As would be expected by analogy with the discussion above of an annual mean Arctic Ocean with a variable sea ice edge, Fig. 2a illustrates that when ΔF_0 becomes sufficiently large that the ocean can remain perennially ice-free with $\alpha = \alpha_{ml}$, a regime with unstable partial-year sea ice (red dashed curve) appears in a saddle-node bifurcation of cycles (See Strogatz[20] for a discussion of the theory of bifurcations in periodic systems). The unstable solution separates stable solutions with perennial ice (blue curve) or open water (black curve). The perennial ice regime collides with the unstable state and disappears in a second saddle-node bifurcation of cycles at the point where ΔF_0 becomes sufficiently large that the ice completely melts at the time of annual maximum E in the cold stable state. Due to the fact that there is significant incident solar radiation during both the maximum and minimum periods of the seasonal cycle of E, the ice-albedo feedback ensures that all solutions with partial-year ice cover will be unstable.

When nonlinear sea ice thermodynamic effects are included (equations (2)-(4)), basal ice formation is controlled by a diffusive vertical heat flux of $k_i \Delta T / h_i$, where ΔT is the difference between surface and basal temperatures. This causes thin ice to grow significantly faster than thick ice[17]. It would also cause thin ice to experience greater basal melt during the summer melt season, but the surface temperature only warms until it reaches the freezing point ($\Delta T = 0$) and surface melt begins, making the rate of melt less sensitive to thickness. These two effects, both nonlinear in E, are expressed in equation (3) by the $1/E$ term in the denominator and the ramp function, respectively. The result is an increase in the rate of growth for thin ice which is more stabilizing for thinner ice, as pointed out[21] and applied[22] in previous studies. This is in contrast to the state-independent linear mixed layer stabilizing term $-F_T(t)E/c_{ml}H_{ml}$ when $E > 0$ (equations (2) and (3)).

These nonlinearities allow for the existence of a stable seasonally ice-free solution (Fig. 2b). When ΔF_0 reaches a value that causes the cold solution to become ice-free during a small part of the year, a slight increase in temperature would lead to a longer open water period and a thinner partial-year ice cover. Although the increased period of open water promotes warming through the ice-albedo feedback, the thinner ice grows significantly faster because of the sea ice thermodynamic effects which are nonlinear in E. During the ice-covered portion of the year, the stability of the solution is controlled by this strong nonlinear stabilizing effect, but during the ice-free portion of the year it is replaced by the the weaker linear mixed layer stabilizing term. This causes the stabilizing sea ice thermodynamic effects to dominate the destabilizing ice-albedo feedback and allow a stable seasonally ice-free solution only when there is ice cover during a sufficiently long portion of the year. Nonetheless, the ice–albedo feedback causes this regime to warm at an increased rate in response to increasing heat flux (compare slopes of red and blue curves in Fig. 2b). As the ice-covered fraction of the year decreases in a warming climate, the stabilizing ice thermodynamic effects become less pronounced, and a bifurcation occurs when ice covers the Arctic Ocean during a sufficiently small fraction of the year to allow the ice-albedo feedback to dominate. Hence when the Arctic warms beyond this point, the system (Fig. 2b) only supports an ice-free solution.

The theoretical treatment presented here is constructed to be readily accessible to conceptual interpretation, and to this end many processes have been neglected. Factors including possible sea ice–cloud feedbacks[23–28], the dependence of sea ice surface albedo on snow and melt pond coverage[29], ocean heat flux convergence feedbacks[6,7], changes in wind-driven ice dynamics[8], and changes in ice rheology[30] in a thinning ice cover[31] could potentially lead to other bifurcation thresholds or remove the threshold investigated here. We are emboldened in our approach, however, because behavior consistent with the mechanism proposed here can be found in the previously published results of models with a wide range of complexities. *(i)* A "toy model" which is forced by a step function seasonal cycle produced no stable seasonally ice-free solution in the standard case parameter regime[32], but by a slight adjustment of the tunable parameters one can find a stable seasonally ice-free solution which coexists with a stable perennial open water solution (Supplementary Fig. S1), consistent with the findings presented here. *(ii)* In a variant of the model used in this study that represents the simultaneous evolution of Arctic sea ice area, mean thickness, surface temperature, and ocean mixed layer temperature, increasing the level of greenhouse gas forcing leads to a gradual transition to seasonally ice-free steady-state solutions before a bifurcation threshold is crossed in the transition to perennially ice-free conditions[33]. *(iii)* Turning to significantly more complex models, about half of the coupled atmosphere–ocean global climate models used for the most recent IPCC report[34] predict seasonally ice-free Arctic Ocean conditions by the end of the 21st century, and none predict perennial open water conditions by the end of the 21st century. However, perennially ice-free Arctic Ocean conditions occur in two of the model simulations after CO_2 quadrupling. Neither model exhibits an abrupt transition when the annual minimum ice cover disappears, but after further warming one of the models abruptly loses its March ice cover when it becomes perennially ice-free[7]. The physical mechanism presented here may help explain this abrupt loss of simulated March ice while simulated September ice receded gradually.

In conclusion, our analysis suggests that a sea ice bifurcation threshold caused by the ice-albedo feedback is not expected to occur in the transition from current perennial ice conditions to a seasonally ice-free Arctic Ocean, but that a bifurcation threshold associated with the sudden loss of the seasonal ice cover may occur in response to further heating. This

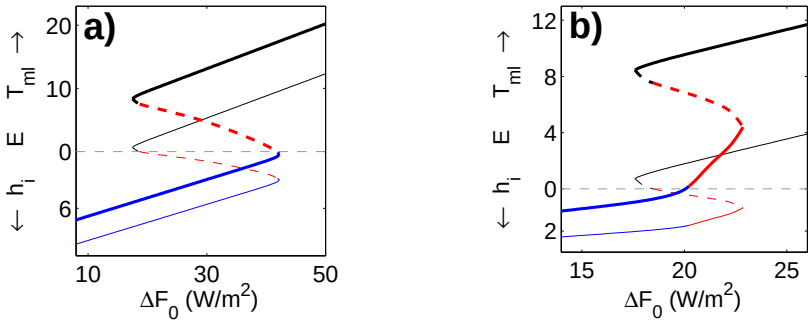

Figure 2: Stable and unstable solutions with (a) linearized ice thermodynamics and (b) full nonlinear ice thermodynamics. The annual maximum (thick curve) and annual minimum (thin curve) value of the seasonally varying model state E is plotted as a function of surface heating ΔF_0. Solutions with perennial ice cover are indicated in blue, seasonally ice-free solutions in red, and perennial ice-free solutions in black. Dashed lines indicate unstable solutions, which have been located by constructing an annual Poincaré map and finding the fixed points, and a small level of noise associated with numerical integration has been smoothed with a boxcar filter. Vertical tick marks are labeled as in Fig. 1a.

conclusion is based on the asymmetry between these two transitions, which both occur during periods of similar incident solar radiation, associated with the fundamental nonlinearities of sea ice thermodynamic effects. As in any study of the fundamental physical processes underlying climate change, the relevance to actual future climate evolution must be carefully qualified. Since the time scale associated with sea ice response to a change in forcing may be decadal (perhaps adjusted significantly because of the role played by the ocean and wind forcing), and the time scale associated with increasing greenhouse gas concentrations may be similar, assessing the stability of a secular base state may be more realistic. Hence in the gradual approach to steady-state under a continual change in forcing, with the high level of variability typical of Arctic sea ice, the difference between a steeply curved region of the steady-state solution and an actual discontinuous bifurcation threshold (as in Fig. 2b) could be difficult to discern. If greenhouse gas concentrations were reduced after crossing a bifurcation threshold, however, the irreversibility of the trajectory would certainly be expected to be relevant.

1. Stroeve, J. C. *et al.* Tracking the Arctic's shrinking ice cover: Another extreme September minimum in 2004. *Geophys. Res. Lett.* **32** (2005).
2. Perovich, D. K. *et al.* Increasing solar heating of the Arctic Ocean and adjacent seas, 1979-2005: Attribution and role in the ice-albedo feedback. *Geophysical Research Letters* **34** (2007).
3. Lindsay, R. W. & Zhang, J. The thinning of Arctic sea ice, 1988-2003: Have we passed a tipping point? *Journal of Climate* **18**, 4879–4894 (2005).
4. Overpeck, J. *et al.* Arctic system on trajectory to new, seasonally ice-free state. *EOS* **86**, 309–313 (2005).
5. Serreze, M. C. & Francis, J. A. The Arctic amplification debate. *Climatic Change* **76**, 241–264 (2006).
6. Holland, M. M., Bitz, C. M. & Tremblay, B. Future abrupt reductions in the summer Arctic sea ice. *Geophysical Research Letters* **33** (2006).
7. Winton, M. Does the arctic sea ice have a tipping point? *Geophys. Res. Lett.* **33**, 10.1029/2006GL028017 (2006).
8. Maslanik, J. *et al.* A younger, thinner arctic ice cover: Increased potential for rapid, extensive sea-ice loss. *Geophys. Res. Lett.* **34**, L24501, doi:10.1029/2007GL032043 (2007).
9. Stroeve, J. *et al.* Arctic sea ice extent plummets in 2007. *Eos Trans. Am. Geophys. Union* **89**, 13–14 (2008).
10. Merryfield, W., Holland, M. & Monahan, A. Multiple equilibria and abrupt transitions in Arctic summer sea ice extent. In Bitz, C. & DeWeaver, E. (eds.) *Arctic Sea Ice Decline: Observations, Projections, Mechanisms, and Implications*, Submitted (American Geophysical Union, 2008).
11. Budyko, M. I. The effect of solar radiatin variations on the climate of the earth. *Tellus* **21**, 611–619 (1969).
12. Sellers, W. D. A global climate model based on the energy balance of the earth-atmosphere system. *J. Appl. Meteor.* **8**, 392–400 (1969).
13. North, G. R. Multiple solutions in energy-balance climate models. *Global and Planetary Change* **82**, 225–235 (1990).
14. Maykut, G. A. & Church, P. E. Radiation climate of Barrow, Alaska, 1962-66. *Journal of Applied Meteorology* **12**, 620–628 (1973).
15. Kalnay, E. *et al.* The NCEP/NCAR 40-year reanalysis project. *Bulletin of the American Meteorological Society* **77**, 437–471 (1996).
16. Nakamura, N. & Oort, A. H. Atmospheric heat budgets of the polar-regions. *Journal of Geophysical Research-atmospheres* **93**, 9510–9524 (1988).
17. Maykut, G. A. & Untersteiner, N. Some results from a time-dependent thermodynamic model of sea ice. *J. Geophys. Res.* **76**, 1550–1575 (1971).
18. Kwok, R., Cunningham, G. F. & Pang, S. S. Fram strait

sea ice outflow. *Journal of Geophysical Research-oceans* **109** (2004).

19. Lenton, T. M. *et al.* Tipping elements in the Earth's climate system. *Proceedings of the National Academy of Sciences* **105**, 1786–1793 (2008).
20. Strogatz, S. H. *Nonlinear Dynamics and Chaos* (Perseus Books, 2001).
21. Maykut, G. The surface heat and mass balance. In Untersteiner, N. (ed.) *The geophysics of sea ice* (Plenium, 1986).
22. Bitz, C. M. & Roe, G. H. A mechanism for the high rate of sea ice thinning in the arctic ocean. *Journal of Climate* **17**, 3623–3632 (2004).
23. Kellogg, W. W. Climatic feedback mechanisms involving the polar regions. In Weller, G. & Bowling, S. A. (eds.) *Climate of the Arctic*, 111–116 (Geophysical Institute, University of Alaska Fairbanks, 1975).
24. Panel on Climate Change Feedbacks. *Understanding Climate Change Feedbacks* (National Academies Press, 2003).
25. Vavrus, S. The impact of cloud feedbacks on arctic climate under greenhouse forcing. *Journal of Climate* **17**, 603–615 (2004).
26. Abbot, D. S. & Tziperman, E. A high latitude convective cloud feedback and equable climates. *Quarterly journal of the Royal Meteorological Society* **134**, 165–2184 (2008).
27. Abbot, D. S. & Tziperman, E. Sea ice, high-latitude convection, and equable climates. *Geophysical Research Letters* **35** (2008).
28. Abbot, D. S. & Tziperman, E. Winter Arctic sea ice uncertainty under global warming due to a cloud radiative feedback. *Submitted (Nature)* (2008).
29. Curry, J. A., Schramm, J. L. & Ebert, E. E. Sea-ice albedo climate feedback mechanism. *Journal of Climate* **8**, 240–247 (1995).
30. Zhang, J. L. & Rothrock, D. A. Effect of sea ice rheology in numerical investigations of climate. *Journal of Geophysical Research-oceans* **110** (2005).
31. Rothrock, D., Percival, D. B. & Wensnahan, M. The decline in Arctic sea-ice thickness: separating the spatial, annual, and interannual variability in a quarter century of submarine data. *Journal of Geophysical Research* in press (2008).
32. Thorndike, A. S. A toy model linking atmospheric thermal radiation and sea ice growth. *J. Geophys. Res.* **97**, 9401–9410 (1992).
33. Eisenman, I. Arctic catastrophes in an idealized sea ice model. In *2006 Program of Studies: Ice (Geophysical Fluid Dynamics Program)*, 133–161 (Woods Hole Oceanog. Inst. Tech. Rept. 2007-02, 2007). Http://gfd.whoi.edu/page.do?pid=12938.
34. Solomon, S. *et al.* (eds.) *Climate change 2007: The Physical Science Basis. Contribution of Working Group I to the Fourth Assessment Report of the Intergovernmental Panel on Climate Change* (Cambridge University Press, Cambridge, UK, 2007).

Acknowledgments The authors are grateful to the Geophysical Fluid Dynamics summer program at Woods Hole Oceanographic Institution (NSF OCE0325296) where the development of the physical representations employed in this study benefited from discussions with many visitors and staff including Norbert Untersteiner, John Walsh, Jamie Morison, Dick Moritz, Danny Feltham, Göran Björk, Bert Rudels, Doug Martinson, Andrew Fowler, George Veronis, Grae Worster, Neil Balmforth, Ed Spiegel, Joe Keller, and Alan Thorndike. IE thanks Eli Tziperman and Cecilia Bitz for helpful conversations during the course of this work. JSW acknowledges support from NSF OPP0440841 and Yale University. IE acknowledges support from a NASA Earth and Space Science Fellowship, a WHOI Geophysical Fluid Dynamics Fellowship, NSF Climate Dynamics program grant ATM-0351123, and the McDonnell Foundation.

Supplementary Information

1 Supplementary Figure

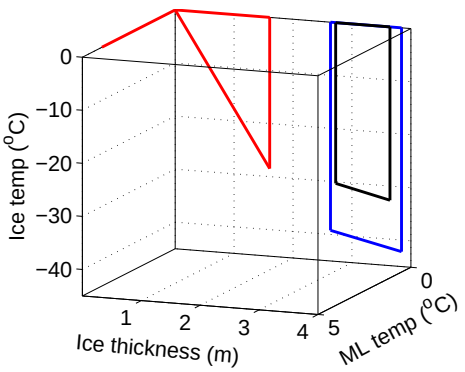

Figure S1: Seasonal cycle of Arctic sea ice and ocean conditions simulated with the toy model of Thorndike[1]. Seasonally varying solutions are plotted as closed curves in the three-dimensional model state space, which represents changes in sea ice thickness, sea ice surface temperature, and mixed layer temperature. The standard case solution is given by the black curve. Thorndike found that when the specified atmosphere Arctic heat flux convergence D was increased, the model transitioned from perennial ice-covered to perennial ice-free conditions, with no stable seasonally ice-free solution possible. Rather than prescribing observed seasonally varying forcing quantities, Thorndike assumes a step-function form for the forcing, with shortwave radiation and optical thickness taking on constant values during the summer and winter half-years. He found observationally consistent ice thickness with the summer and winter optical thicknesses of 4.5 and 3, respectively. When we chose for these parameters instead 1.5 and 5, respectively, Thorndike's toy model simulates a relatively consistent approximation of the modern sea ice seasonal cycle (blue curve). Increasing D from 100 to 145 W/m^2 in this regime, however, produces a stable seasonally ice-free solution (red curve). A second stable state which is perennially ice-free exists for the solution indicated by the black curve, as discussed by Thorndike, but not for the solution shown by the blue curve. A second stable state which is perennially ice-free does however exist for the solution indicated by the red curve. The coexistence in Thorndike's model of a stable seasonally ice-free solution and a stable perennially ice-free solution is consistent with the results of the model presented here illustrated in Fig. 2.

2 Supplementary Methods: Model Derivation

Here we derive the idealized Arctic sea ice–ocean–atmosphere model summarized in equations (1)-(4) of the Letter.

Sea ice The evolution of the sea ice temperature T is an idealized version of the single-column thermodynamic model of Maykut & Untersteiner[2] (hereafter MU71). Vertical heat conduction in sea ice is computed in MU71 according to

$$c_{\text{eff}}(T,S)\frac{\partial T}{\partial t} = k_{\text{eff}}(T,S)\frac{\partial^2 T}{\partial z^2} + A_R, \qquad \text{(S1)}$$

which can be derived from the general theory of mushy layers[3]. Here A_R represents the absorption of shortwave radiation that has penetrated below the surface of the ice, the effective heat capacity $c_{\text{eff}}(T,S)$ and thermal conductivity $k_{\text{eff}}(T,S)$ depend on simulated temperature T and specified salinity S, and the vertical coordinate z increases upward. For the T and S range in perennial ice MU71 neglected the vertical derivative of the effective conductivity, $\partial k_{\text{eff}}(T,S)/\partial z$. MU71 include a layer of snow above the ice with specified snowfall and simulated snow melt. Here we also neglect snow (MU71 report that having no snow causes the annual mean thickness to increase by 17cm from the standard case value of 288cm), and we neglect penetrating shortwave radiation (which MU71 report causes the annual mean ice thickness to decrease by 45cm). The impacts of neglecting these factors is shown in Fig. S2 (gray and black curves).

The boundary condition in MU71 at the upper surface, $z = h_T$, is a flux balance when the ice is below the freezing temperature (T_{fr}) and otherwise a Stefan condition for surface ablation:

$$k_{\text{eff}}(T,S)\left[\frac{\partial T}{\partial z}\right]_{h_T} + F_{top}(t,T_i,\alpha_i) = \begin{cases} 0 & T_i < T_{fr} \\ L_{\text{i}}\frac{dh_T}{dt} & T_i = T_{fr} \end{cases}. \qquad \text{(S2)}$$

Here $F_{top}(t,T_i,\alpha_i)$ represents the sum of sensible, latent, longwave, and shortwave heat fluxes out of the surface. The seasonal cycle of each of these components of the surface flux are specified in MU71 based on observations, except for the upward longwave flux which is computed from the surface temperature, $T_i \equiv [T]_{h_T}$, using the Stefan-Boltzmann equation. To facilitate an analytical solution for T_i (equation (S13) below), here we approximate the Stefan-Boltzmann equation by its linearized version, $\sigma(T_i+T_{fr})^4 \approx (\sigma_0 + \sigma_T T_i)$, where the temperature T_i is written in terms of the departure from the freezing point (e.g., °C), σ is the Stefan-Boltzmann constant, and σ_0 and σ_T are chosen such that the equation is exact when $T_i = -30°$and when $T_i = 0°$C (the approximate values of T_i during most of the winter and summer, respectively).

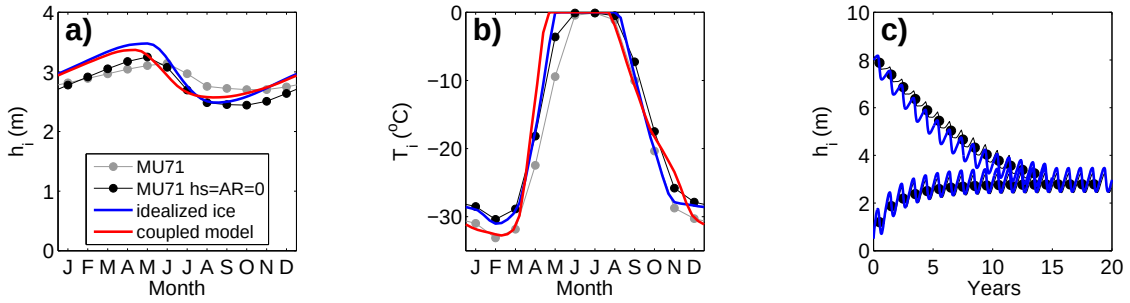

Figure S2: Effects of approximating the ice thermodynamics in the model of MU71 [2]. (a) Steady-state solution seasonal cycle of ice thickness in the MU71 standard case simulation (gray curve and circles), in a simulation with the MU71 model with no snow or penetrating shortwave radiation ($h_s = A_R = 0$; black curve and circles), the effect of replacing the MU71 representation with the idealized sea ice model given by equations (S13)-(S14) (blue curve), and the standard case run with the fully coupled idealized sea ice–ocean–atmosphere model summarized in equations (1)-(4) in the Letter (red curve). (b) Seasonal cycle of surface temperature for the same four simulations as in (a). (c) Relaxation time to reach steady-state ice thickness from two different initial conditions for the MU71 model with $h_s = A_R = 0$ (black curves and circles) and the idealized sea ice model (blue curves).

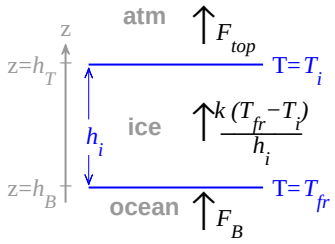

Figure S3: Schematic showing fluxes and variables in the sea ice component of the idealized model. All fluxes defined such that a positive value implies an upward flux.

This allows us to express the surface flux as

$$F_{top}(t,T,\alpha) = F_0(t) - (1-\alpha)F_S(t) + F_T(t)T. \qquad \text{(S3)}$$

At the base of the ice layer, $z = h_B$, MU71 apply a Stefan condition for ice growth or ablation,

$$-\left[k_{\text{eff}}(T,S)\frac{\partial T}{\partial z}\right]_{h_B} - F_B = -L_i\frac{dh_B}{dt}, \qquad \text{(S4)}$$

with the flux from the ocean into the base of the ice specified in MU71 to take a constant value of $F_B = 2$ W/m^2. The temperature at the ice–ocean interface must be equal to the freezing temperature, $[T]_{h_B} = T_{fr}$. The upper and lower surfaces of the ice, h_T and h_B, are evolved separately, and the predicted ice thicknesses is $h_i = h_T - h_B$ (Fig. S2).

The relatively large Stefan number, $N_S \equiv L_i/(c_{\text{eff}}\Delta T)$, facilitates the integration of equation (S1) because the solidification rate is sufficiently small that the temperature field in the ice relaxes quickly. The predicted seasonal cycle in MU71 implies values of N_S which range widely but typically are $N_S \gg 1$. The thermal conductivity $k_{\text{eff}}(T,S)$ in the MU71 standard run is always 90%–100% of the pure ice value, and we approximate $k_{\text{eff}}(T,S)$ to take the constant pure ice value, $k_i = 2$ W/m/K. The freezing temperature in MU71 is taken to be $T_{fr} = -1.8°$C at the base of the ice and $T_{fr} = -0.1°$C at the upper ice surface, and we approximate it to take a constant value of $T_{fr} = 0°$C. Under these approximations, the integral of the left hand side of equation (S1) can be written

$$\int_{h_B}^{h_T} dz\left(c_{\text{eff}}(T,S)\frac{\partial T}{\partial t}\right) \approx \frac{c_{\text{eff}}h_i}{2}\frac{dT_i}{dt}, \qquad \text{(S5)}$$

where the large Stefan number assumption has allowed us to assume that the temperature field is quasi-stationary, hence satisfying a linear profile, $T = (T_i - T_{fr})(z - h_B)/(h_T - h_B)$. Applying the same integration to the right hand side of equation (S1) leads to an approximate representation of vertical heat conduction in the sea ice,

$$\frac{c_{\text{eff}}h_i}{2}\frac{dT_i}{dt} = k_i\left[\frac{\partial T}{\partial z}\right]_{h_T} - k_i\left[\frac{\partial T}{\partial z}\right]_{h_B}. \qquad \text{(S6)}$$

Next we insert the boundary conditions (S2) and (S4) into equation (S6), which leads to two sets of equations depending on whether or not surface ablation is occurring. In either case, the linear internal temperature gradient is used for the lower boundary term ($k\left[\partial T/\partial z\right]_{h_B} = k_i T_i/h_i$) because of the Stefan condition at the base, and the lower boundary condition (S4) becomes

$$-L_i\frac{dh_B}{dt} = -k_i\frac{T_i}{h_i} - F_B. \qquad \text{(S7)}$$

When $T_i < T_{fr}$, the first upper boundary condition in equation (S2) gives $k_i\left[\partial T/\partial z\right]_{h_T} = -F_{top}(t,T_i,\alpha_i)$. Inserting this into (S6) and using $dh_i/dt = d/dt\,(h_T - h_B) = -dh_B/dt$ in (S7) leads to

$$\frac{c_{\text{eff}}h_i}{2}\frac{dT_i}{dt} = -F_{top}(t,T_i,\alpha_i) - k_i\frac{T_i}{h_i}, \qquad \text{(S8)}$$

$$L_i \frac{dh_i}{dt} = -k_i \frac{T_i}{h_i} - F_B. \tag{S9}$$

When $T_i = T_{fr}$, the Stefan condition at the upper edge leads to the use of the internal temperature gradient for the upper boundary term, $k_i \left[\partial T/\partial z\right]_{h_T} = k_i T_i/h_i$. Using the second upper boundary condition in equation (S2), $L_i dh_T/dt = k_i T_i/h_i + F_{top}(t, T_i, \alpha_i)$, equations (S6) and (S7) become

$$\frac{dT_i}{dt} = 0, \tag{S10}$$

$$L \frac{dh_i}{dt} = F_{top}(t, T_i, \alpha_i) - F_B. \tag{S11}$$

The large Stefan number approximation can be now expressed in terms of the surface temperature T_i being in approximate steady-state with the more slowly evolving ice thickness, $dT_i/dt = 0$ in equation (S8). Inserting equation (S3), under this approximation equation (S8) can be written

$$0 = F_0(t) - (1-\alpha)F_S(t) + F_T(t)T_i + k_i \frac{T_i}{h_i}. \tag{S12}$$

Solving equation (S12) T_i and combining this with equation (S10) gives a single equation for the surface temperature,

$$T_i(t, h_i) = -\mathcal{R}\left(\frac{F_0(t) - (1-\alpha_i)\,F_S(t)}{F_T(t) + k_i/h_i}\right), \tag{S13}$$

where the ramp function $\mathcal{R}(x)$ is 0 if $x < 0$ and $\mathcal{R}(x) = x$ if $x > 0$. Note that the two branches of the ramp function have arisen as a result of the two surface boundary conditions in equation (S2). Inserting equation (S12) into equation (S9) allows equations (S9) and (S11) to be combined in the form of equation (S11),

$$L_i \frac{dh_i}{dt} = F_0(t) - (1-\alpha_i)F_S(t) + F_T(t)T_i(t, h_i) - F_B. \tag{S14}$$

The sea ice model is fully contained in equations (S13)-(S14). The results of the idealized ice model forced by specified surface and basal fluxes as in MU71 are shown in Fig. S2 (blue curves), and the ice model fluxes are illustrated schematically in Fig. S3.

While most aspects of ice dynamics are neglected in this idealized treatment, in the coupled version of the model we parameterize the net annual export of sea ice out of the central Arctic, most of which escapes through Fram Straight. Arctic sea ice has a residence time of roughly 3-12 years [4], with a net annual export of about 10% of the ice area[5]. This continuous export of ice makes the ice thickness somewhat more stable: to maintain thicker ice, a larger amount of new ice must be produced each year. We approximately account for this by adding to the ice thickness evolution (S14) a decay term $-v_0 L_i h_i$, with $v_0 = 0.1$ year^{-1}.

Atmosphere In the presence of significantly different Arctic Ocean surface conditions, such as an exposed ocean mixed layer, the atmospheric heat fluxes into the surface are expected to change substantially. This is particularly true for the downwelling longwave radiation which includes contributions from both horizontal atmospheric heat flux convergence and downward re-emission of upward longwave radiation due to the opacity of the atmosphere (i.e., the greenhouse effect). Here we approximately compute downwelling longwave radiation using an idealized atmospheric model.

The meridional heat flux convergence averaged over 70°N–90°N is equivalent to a spatially averaged vertical flux of roughly $D = 100$ W/m^2 [6]. Since the poleward heat flux in the atmosphere is related to mixing of sensible and latent heat by eddies, it is often approximated in idealized climate models as being proportional to the meridional temperature difference[7–9], which is equivalent to assuming meridional effective diffusion of temperature as in typical atmospheric energy balance models[10–12]. Although a destabilizing increase in atmospheric meridional heat flux into the Arctic may occur in response to warming due to factors including increased humidity[13–16], when the warming is significant a principal damping mechanism is expected to be reduced atmospheric heat transport[17], and we follow the convention of setting the meridional heat flux to be proportional to the merdional temperature difference,

$$D(t, T) = k_D \Delta T_{merid}(t). \tag{S15}$$

Here $\Delta T_{merid} = T_{south}(t) - T$ with T the simulated surface temperature in the Arctic and $T_{south}(t)$ the seasonally varying temperature south of the Arctic which is specified here from NCEP-NCAR reanalysis 1971-2000 climatological 1000mb atmospheric temperature[18] spatially averaged in the region 0°–70°N. We use $k_D = 2.7$ W/m^2/K, which optimizes the match to observed poleward heat transport[6] (although this parameterization leads to a model annual cycle in D that is somewhat exaggerated compared to observations). We assume that half the heat flux convergence is radiated upward to space and half contributes to the downward longwave radiative flux at the surface[1].

The effect of a vertically continuous dry radiative two-stream grey-absorbing non-scattering energy balance atmospheric model on the surface longwave flux balance is fundamentally to mitigates surface longwave cooling by reemitting some of the heat back to the surface. It can be shown to lead to a net surface longwave flux equivalent to scaling the upward longwave radiation by $\kappa_{LW} < 1$, where κ_{LW} is inversely related to a linear function of the atmospheric optical thickness and hence depends on water vapor, cloud particles, and greenhouse gases such as carbon dioxide[1,19,20]. We specify the optical thickness seasonal cycle to follow observed Arctic cloudiness,

$$\kappa_{LW}(t) = \frac{1}{\tau_0 + \tau_c f_c(t)}, \tag{S16}$$

where $f_c(t)$ is the Arctic cloud fraction seasonal cycle specified from observations[21] and τ_0 and τ_c are chosen to give a sea ice seasonal cycle matching that computed using forcing from MU71.

The actual heat flux at the top of the sea ice or exposed ocean mixed layer, $F_{top}(t, T, \alpha)$, includes components of sensible and latent heat fluxes in addition to downward and upward shortwave and longwave radiations. According to the observationally based central Arctic values specified in MU71, the sensible and latent heat fluxes are small compared to the radiative fluxes, and here we effectively approximate the sensible and latent heat fluxes by incorporating them into the computed downwelling longwave flux. The longwave emissivities of ice and open water, both roughly 0.95–1, are here approximated to unity. Under these approximations, the total surface flux can be written

$$F_{top}(t,T,\alpha) = \kappa_{LW}(t)\,(\sigma_0 + \sigma_T T) - \frac{D(t,T)}{2} - (1-\alpha)F_S(t), \tag{S17}$$

where the downwelling shortwave radiation incident at the surface, $F_S(t)$, is specified from observations as in MU71. Inserting (S15) and (S3), we can write the components of the surface flux as

$$F_0(t) = \kappa_{LW}(t)\sigma_0 - \frac{k_D}{2}T_{south}(t) \tag{S18}$$

and

$$F_T(t) = \kappa_{LW}(t)\sigma_T + \frac{k_D}{2}. \tag{S19}$$

Ocean mixed layer To allow the simulation of ice-free conditions, we include a representation of an ocean mixed layer which becomes exposed when all of the ice ablates. The mixed layer is represented as a thermodynamic reservoir with a characteristic depth of $H_{ml} = 50$m, in agreement with observations[22]. The mixed layer temperature evolves according to

$$c_{ml}H_{ml}\frac{dT_{ml}}{dt} = (1-\alpha_{ml})\,F_S(t) - F_0(t) - F_T(t)T_{ml} + F_B, \tag{S20}$$

with mixed layer heat capacity $c_{ml} = 4 \times 10^6$ J/m^3/K. We use an open water albedo of $\alpha_{ml} = 0.2$, similar to previous studies[1,23], to account for the presence of small amounts of thin ice in a largely ice-free Arctic Ocean. When $h_i = 0$, the mixed layer temperature is evolved forward from $T_{ml} = 0$, and when the mixed layer cools back to the freezing point the ice thickness is evolved once again starting from $h_i = 0$.

Coupled model The separate equations for T_{ml} and h_i can be combined, since only one is evolving at any given time. We define the energy per unit area in the system, E, to be equal to the sum of the latent heat content of the sea ice and the specific heat content of the mixed layer (equation (1) in main text). This allows the ice and mixed layer components of the idealized model (S13)-(S20) to be expressed as equations (2)-(4) in the Letter.

The model presented in this paper is completely specified by equations (1)-(4) with the parameter values given in Table S1. The parameters $F_0(t)$ and $F_T(t)$, which are used to determine the surface heat flux, have values that were computed using the atmospheric model (S18)-(S19). Time evolution t is measured in years, while fluxes are measured in W/m^2, which conveniently allows most dimensional parameters to be approximately of order unity but requires a non-conventional choice of units for energy per unit area E (written in W/m^2 yr), heat capacity $c_{ml}H_{ml}$, latent heat L_i.

1. Thorndike, A. S. A toy model linking atmospheric thermal radiation and sea ice growth. *J. Geophys. Res.* **97**, 9401–9410 (1992).
2. Maykut, G. A. & Untersteiner, N. Some results from a time-dependent thermodynamic model of sea ice. *J. Geophys. Res.* **76**, 1550–1575 (1971).
3. Feltham, D. L., Untersteiner, N., Wettlaufer, J. S. & Worster, M. G. Sea ice is a mushy layer. *Geophys. Res. Lett.* **33** (2006).
4. Rigor, I. G. & Wallace, J. M. Variations in the age of Arctic sea-ice and summer sea-ice extent. *Geophys. Res. Lett.* **31** (2004).
5. Kwok, R., Cunningham, G. F. & Pang, S. S. Fram strait sea ice outflow. *Journal of Geophysical Research-oceans* **109** (2004).
6. Nakamura, N. & Oort, A. H. Atmospheric heat budgets of the polar-regions. *Journal of Geophysical Research-atmospheres* **93**, 9510–9524 (1988).
7. Chen, D., Gerdes, R. & Lohmann, G. A 1-D atmospheric energy-balance model developed for ocean modeling. *Theoretical and Applied Climatology* **51**, 25–38 (1995).
8. Thorndike, A. A minimal model of sea ice and climate. In Wettlaufer, J. S., Dash, J. G. & Untersteiner, N. (eds.) *Ice Physics and the Natural Environment*, 169–183 (Springer-Verlag, 1999).
9. Gildor, H. & Tziperman, E. A sea-ice climate-switch mechanism for the 100 kyr glacial cycles. *J. Geophys. Res.* **106**, 9117–9133 (2001).
10. Budyko, M. I. The effect of solar radiatin variations on the climate of the earth. *Tellus* **21**, 611–619 (1969).
11. Sellers, W. D. A global climate model based on the energy balance of the earth-atmosphere system. *J. Appl. Meteor.* **8**, 392–400 (1969).
12. North, G. R., Cahalan, R. F. & Coakley, Jr., J. A. Energy balance climate models. *Rev. Geophys. Space. Phys.* **19**, 91–121 (1981).
13. Alexeev, V. A. Sensitivity to CO_2 doubling of an atmospheric GCM coupled to an oceanic mixed layer: a linear analysis. *Climate Dynamics* **20**, 775–787 (2003).
14. Hall, A. The role of surface albedo feedback in climate. *Journal of Climate* **17**, 1550–1568 (2004).
15. Winton, M. Amplified arctic climate change: What does surface albedo feedback have to do with it? *Geophysical Research Letters* **33** (2006).
16. Held, I. M. & Soden, B. J. Robust responses of the hydrological cycle to global warming. *Journal of Climate* **19**, 5686–5699 (2006).
17. Winton, M. Sea ice-albedo feedback and nonlinear arctic climate change. In Bitz, C. & DeWeaver, E. (eds.) *Arc-*

Symbol	Description	Value
L_i	Latent heat of fusion of ice	9.5 W/m^2 yr/m
$c_{ml}H_{ml}$	Mixed layer heat capacity times depth	6.3 W/m^2 yr/K
α_i	Albedo of ice	0.68
α_{ml}	Albedo when ocean mixed layer is exposed	0.2
k_i	Ice thermal conductivity	2 W/m/K
F_B	Heat flux into bottom of ice or ocean mixed layer	2 W/m^2
h_α	Ice thickness range for transition from α_i to α_{ml}	0.5 m
v_0	Dynamic export of ice from model domain	0.10 yr^{-1}
$F_0(t)$	Temperature-independent surface flux	85 W/m^2 (120,120,130,94,64,61,57,54,56,64,82,110)
$F_T(t)$	Temperature-dependent surface flux	2.8 W/m^2/°C (3.1,3.2,3.3,2.9,2.6,2.6,2.6,2.5,2.5,2.6,2.7,3.1)
$F_S(t)$	Incident shortwave radiation flux	100 W/m^2 (0,0,30,160,280,310,220,140,59,6.4,0,0)

Table S1: Descriptions and default values of model parameters. For seasonally varying parameters, the annual mean is given followed by monthly values starting with January listed in parenthesis.

tic Sea Ice Decline: Observations, Projections, Mechanisms, and Implications, Submitted (American Geophysical Union, 2008).

18. Kalnay, E. *et al.* The NCEP/NCAR 40-year reanalysis project. *Bulletin of the American Meteorological Society* **77**, 437–471 (1996).
19. Goody, R. & Yung, Y. *Atmospheric Radiation: Theoretical Basis* (Oxford University Press, 1989), 2 edn.
20. Salby, M. L. *Fundamentals of Atmospheric Physics* (Academic Press, 1996).
21. Maykut, G. A. & Church, P. E. Radiation climate of Barrow, Alaska, 1962-66. *Journal of Applied Meteorology* **12**, 620–628 (1973).
22. Morison, J. & Smith, J. D. Seasonal-variations in the upper Arctic ocean as observed at T-3. *Geophys. Res. Lett.* **8**, 753–756 (1981).
23. Hibler, W. D. A dynamic thermodynamic sea ice model. *J. Phys. Oceanogr.* **9**, 815–846 (1979).